Journal of Power Sources 195 (2010) 7160–7167

Contents lists available at ScienceDirect

Journal of Power Sources

journal homepage: www.elsevier.com/locate/jpowsour

Direct ceramic inkjet printing of yttria-stabilized zirconia electrolyte layers for anode-supported solid oxide fuel cells

R.I. Tomov[a,*], M. Krauz[b], J. Jewulski[c], S.C. Hopkins[a], J.R. Kluczowski[b], D.M. Glowacka[d], B.A. Glowacki[a,c]

[a] Applied Superconductivity and Cryoscience Group, Department of Materials Science and Metallurgy, University of Cambridge, Cambridge CB4 3QZ, UK
[b] Institute of Power Engineering, Ceramic Department CEREL, 36-040 Boguchwała, Poland
[c] Institute of Power Engineering, Fuel Cells Department, 02-981 Warsaw, Poland
[d] Detector Physics Group, Cavendish Laboratory, University of Cambridge, Cambridge CB3 0HE, UK

ARTICLE INFO

Article history:
Received 16 February 2010
Received in revised form 10 May 2010
Accepted 25 May 2010
Available online 31 May 2010

Keywords:
YSZ
Inkjet printing
SOFC
Ceramic
Suspension

ABSTRACT

Electromagnetic drop-on-demand direct ceramic inkjet printing (EM/DCIJP) was employed to fabricate dense yttria-stabilized zirconia (YSZ) electrolyte layers on a porous NiO–YSZ anode support from ceramic suspensions. Printing parameters including pressure, nozzle opening time and droplet overlapping were studied in order to optimize the surface quality of the YSZ coating. It was found that moderate overlapping and multiple coatings produce the desired membrane quality. A single fuel cell with a NiO–YSZ/YSZ (~6 μm)/LSM + YSZ/LSM architecture was successfully prepared. The cell was tested using humidified hydrogen as the fuel and ambient air as the oxidant. The cell provided a power density of 170 mW cm^{-2} at 800 °C. Scanning electron microscopy (SEM) revealed a highly coherent dense YSZ electrolyte layer with no open porosity. These results suggest that the EM/DCIJP inkjet printing technique can be successfully implemented to fabricate electrolyte coatings for SOFC thinner than 10 μm and comparable in quality to those fabricated by more conventional ceramic processing methods.

1. Introduction

Solid oxide fuel cells (SOFC) have attracted increasing attention in recent years due to their high energy conversion efficiency, expected environmental benefits and the flexibility of fuels used. SOFC are based on a variety of ceramic electrolyte coatings conducting oxygen ions and simultaneously being good electrical insulators [1–6]. Currently, fully yttria-stabilized zirconia (YSZ) is the most commonly used electrolyte material for intermediate and high temperature operation (650–1000 °C) due to its unique properties such as excellent mechanical strength, high chemical and thermal stability and pure oxygen ionic conductivity over a wide range of conditions [5,7–9]. A Ni–YSZ anode is preferred for mechanical support in anode-supported SOFC (AS-SOFC) because it provides good electrical conductivity and mechanical strength, as well as minimal chemical interaction with the electrolyte [10]. Running SOFC at high temperatures causes functional material degradation and is detrimental to the durability of the cell. In order to avoid the materials problems significant research effort has been directed towards intermediate temperature SOFC (IT-SOFC) which are to be operated at temperatures of 650–800 °C [11]. IT-SOFC allows the use of ferritic stainless steel for interconnect components, thus reducing the cost, as well as offering improved stability and minimized thermo-mechanical stresses [12]. However, the ionic conductivity of the electrolyte declines with decreasing temperature, which leads to higher ohmic losses. A general approach to solve the problem is the reduction of electrolyte thickness, preferably to below 10 μm, while simultaneously preserving its gas tightness [13–15]. A thinner membrane results in lower ohmic losses during cell operation, effectively reducing the operating temperature of SOFC.

Thin YSZ electrolytes have been successfully prepared by a number of techniques [14] including vapor deposition techniques such as RF magnetron sputtering [16], chemical vapor deposition (CVD) [17] and e-beam deposition [18]. Such processes are not cost-effective and are difficult to scale up. Ceramic powder processing routes like tape-casting [19] and screen printing [20] are widely used and produce excellent coatings. They are inexpensive and readily commercialized, but reliable deposition of coatings with thicknesses less than 10 μm presents a challenge. Liquid phase deposition techniques like spray coating [21], electrostatic spray deposition (ESP) [22], dip coating [23] or spin coating [24] are economical and suitable for preparing thin coatings, but require the deposition of multiple coatings and complex sintering procedures. The major drawback of these techniques is related to the strain induced during thermal cycling, which results in appearance of defects, such as cracks, pores, or delamination.

Inkjet printing has been implemented for the fabrication of coatings and patterns on a variety of surfaces. It can reproducibly

* Corresponding author. Tel.: +44 (0)1223 767933; fax: +44 (0)1223 334567.
E-mail address: rit21@cam.ac.uk (R.I. Tomov).

0378-7753/$ – see front matter © 2010 Elsevier B.V. All rights reserved.
doi:10.1016/j.jpowsour.2010.05.044

dispense droplets of fluid with volumes from several pico-liters to tens of nano-liters at rates of several kHz on demand. Electromagnetic and piezoelectric dispensing technologies are suitable for a wide range of materials including liquid metals, colloidal suspensions, sol inks, sealants and adhesives [25–27]. Some inkjet printing technologies also offer accurate adjustment of the droplet volume and the number of droplets delivered per unit area of substrate, thus controlling the thickness of the layer with precision. The technology is environmentally friendly due to its very low material wastage. Young et al. [28] have successfully demonstrates the use of piezoelectric Dimatix Materials Printer DMP-2831 for fabrication of SOFC. They applied a 20-layer coating, obtaining dense YSZ electrolyte layers 6–12 μm thick. El-Toni et al. [29] successfully demonstrated the utilization of a KEGON-M3 print head (108 mm × 108 mm print size) for printing a $Ce_{0.9}Gd_{0.1}O_{1.95}$ coating on a honeycomb porous LSM substrate, demonstrating the suitability of inkjet printing for the processing of complex SOFC components.

In this paper we are exploring the feasibility of a simpler and more cost-effective direct ceramic inkjet printing method by employing less demanding electromagnetic inkjet technology (EM/DCIJP). We are targeting the production of dense YSZ electrolyte membranes thinner than 10 μm with improved surface flatness on porous NiO/YSZ substrates from ceramic suspensions.

2. Experimental

2.1. Ink preparation and characterization

DCIJP employs inks prepared from ceramic powder suspended in a carrier fluid and dispensed by single- or multiple-nozzle print heads. The preparation of stable suspensions is a paramount factor in achieving repeatable jetting and avoiding clogging of the nozzle. The orifice diameter of the nozzle implemented in this work was 90 μm. In order to avoid the risk of clogging the nozzle one should take care to limit the powder particle size to below the empirically established level of $S < (D_{nozzle}/50) = 1.6$ μm. The ceramic deposition rate is proportional to the powder mass load and limited by the rheological working window of the nozzle which defines the regime of stable repeatable jetting. The particle size of YSZ powders (before and after milling) was measured using a particle size analyzer (Malvern Instruments MasterSizer S, 45 mm focal length). The original powder (ZrO_2–8 mol.% Y_2O_3, Tosoh) mostly consisted of particles and agglomerates up to 20–40 μm in size which tended to dissociate during an ultrasonic bath treatment (L&R Ultrasonicator T14B, 95 W). Two batches of the original powder in methanol were ball milled with 10 mm YSZ beads in YSZ bowls in a Fritsch Pulverizette 7 planetary mill for 1 and 4 h respectively. As milled powders and a batch of the original powder were filtered through 2.7 and 1 μm glass fibre filters and analyzed. Milling for 1 h did not produce a noticeable size difference with the original powder. A bimodal distribution was observed for both batches with almost equal peaks centred at 2 and ~0.4 μm diameter, reflecting the characteristics of the filters used. The filtered powder milled for 4 h was found to consist largely of particles ~0.4 μm in size with a small tail reaching the $S = 1.6$ μm size limit.

All ceramic suspensions in this study were prepared by dispersing ball milled and filtered YSZ powder in alpha-Terpineol which was reported to act efficiently as an ink carrier and a dispersant [30]. The viscosity of the suspensions was adjusted to the levels suitable for the printing nozzles by adding methanol. A mixture of equal parts by weight of bis(2-ethylhexyl)phthalate and ethyl cellulose were also added as a plasticizer and a binder respectively. Several different suspensions were prepared by changing the weight percentage (wt.%) of YSZ powder mass load in the range of 5–15%. The viscosities of 5 and 15 wt.% suspensions were measured with a resonance viscosity meter (Hydramotion Viscolite 700) at high shear rates, revealing values of 2.7 and 4.1 cP respectively. The suspensions prepared with 5 and 15 wt.% powder mass load were sufficiently stable to permit printing without additional mechanical mixing within 72 and 24 h of preparation respectively. The nozzles were observed to execute reproducible drop-on-demand tasks without clogging the internal fluidic pathways of the assembly.

2.2. Anode and cathode preparation

Anode supports for the AS-SOFC cells, approximately 500 μm thick and 57 mm × 57 mm in size, were fabricated using a tape-casting technique. Nickel oxide powder (50 wt.%) and YSZ powder (50 wt.% – 3 mol.% Y_2O_3–ZrO_2) were mixed, and graphite was added as an agent to introduce porosity (25% of the total volume). Finally PVB binder was added (55% of the final mass). The resulting suspension mixture was milled for 48 h in a porcelain ball mill. The suspension was then de-aerated by mixing with low rotating speed (2 revolutions min^{-1}) for 24 h, followed by treatment in vacuum apparatus for 10 min at 0.4 bar pressure. Next the anode support was tape-cast at a speed of ~2 m min^{-1}. Anode support tapes were then dried under ventilation for 12 h, cut out and sintered at 1100 °C.

An interlayer of the same composition was coated on the top of the anode support by screen printing. After drying, it was sintered at 1100 °C. This resulted in a smoother anode surface more suitable as a substrate for inkjet printing.

A composite $La_{0.8}Sr_{0.2}MnO_3$(LSM) + YSZ (50:50 wt.%) interlayer and LSM cathode layer were deposited on the YSZ electrolyte by screen printing. The cathode was sintered at 1100 °C for 2 h in air.

2.3. YSZ electrolyte preparation

The inkjet printer used in this experiment consists of a stationary electromagnetically driven single-nozzle print head with a 90 μm ruby orifice, modified from a Domino Macrojet printer, mounted 4 mm above a substrate positioned by a computer-controlled x–y stage [25–27]. The electromagnetic nozzle was chosen due to its simplicity and reliability of use, larger orifice diameters and a wider range of ink/suspension compatibility than typical piezoelectric ones, for which the operating viscosity and surface tension range is often more restricted. Another important advantage of the electromagnetic nozzle is that it can be readily dismantled and cleaned. Suspensions are delivered under pressure to a reservoir sealed using a rubber-tipped piston (see Fig. 1). As an electrical pulse passes through the solenoid, the electromagnetic field lifts the piston off the inner face of the orifice for a selected amount of time – the "opening time" parameter – and a volume of the suspension is ejected from the nozzle forming a droplet. An advantage of this magnetic/piston mechanism is that the solenoid is separated from the ink/suspension reservoir and therefore little heating occurs, keeping the viscosity of the suspension constant and delaying the effects of agglomeration and sedimentation.

Optimization of the jetting parameters for each suspension was performed with opening times in the 375–550 μs range and at pressures of 0.4–0.8 kg cm^{-2}. After choosing the optimum parameters, complete coatings were printed using a reciprocating raster pattern. One should note that below certain opening times (for pressures of 0.8 and 0.6 kg cm^{-2} this was 375 μs and for a pressure of 0.4 kg cm^{-2} this was 400 μs), it did not appear possible to release individual droplets from the nozzle. In these cases the droplets were so small that, due to capillary action, they hung onto the base of the nozzle and collected until gravitational effects caused the accumulated mass to drop. Opening times longer than 600 μs were avoided

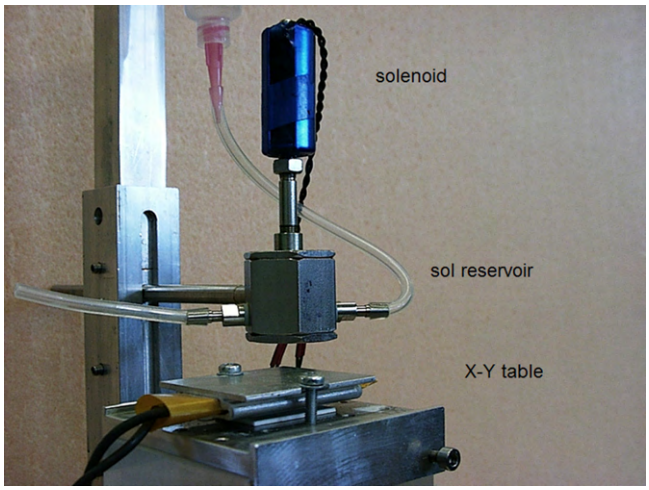

Fig. 1. Annotated photograph of a customised drop-on-demand electromagnetic inkjet print head.

for the reported work as they produced larger droplet volumes less suitable for thin coatings.

The suspensions were deposited on NiO–YSZ ceramic support substrates, which had been prepared by tape-casting as described above. In order to optimize the jetting parameters for each suspension, tests were performed with opening times at 25 μs intervals in the 375–550 μs range and at pressures of 0.4, 0.6 and 0.8 kg cm^{-2}. Five droplets were printed for each combination of opening time and pressure, and then sintered at 1100 °C. Optical micrographs were obtained for each resulting droplet 'relic' on the substrate. These images were processed to produce evenly-illuminated greyscale images, individually thresholded to produce binary images, and analyzed using ImageJ software to characterize the relic sizes and shapes.

The effect of varying the overlapping percentage and the number of layers on surface morphology was investigated. A schematic diagram of a hexagonal grid of droplets with the minimum 25% overlapping required for complete coverage is shown in Fig. 2. The overlapping percentage H was defined as the ratio of the vertical overlap h to the diameter of a single droplet D ($H = h/D$). Subsequent layers were added on top of each other.

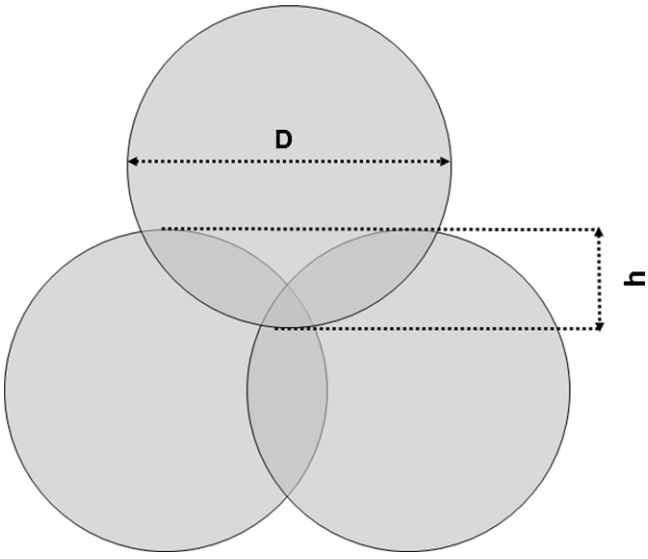

Fig. 2. Schematic showing overlap between droplets in a hexagonal grid for the minimum overlap providing complete coverage. This minimum overlapping percentage (H) is $H_{min} = h/D = 25\%$.

Dark field and bright field optical microscopy as well as mechanical stylus profilometry (Veeco Dektak 3ST) were used to confirm the macroscopic quality of the surface and the completeness of the coverage. The density and the thickness of the sintered coatings on the microscopic level were evaluated by cross-sectional SEM imaging.

After choosing the optimum parameters, complete coatings were printed on the 57 mm × 57 mm square NiO–YSZ ceramic supports using a hexagonal array of droplets printed in reciprocating raster pattern. As-prepared single fuel cells were tested in a specially developed ceramic enclosure. The tests were performed at 700, 750 and 800 °C using humidified hydrogen as the fuel (at a constant flow rate of 200 ml min^{-1}) and ambient air as the oxidant.

3. Results and discussion

3.1. Printing parameters optimization

Spreading of the ceramic suspension droplets on the substrate is a function of the rheological ink parameters and interfacial interaction between the droplet and the substrate. The spreading of droplets on porous surface is driven by inertia and capillary forces. A spreading mechanism driven only by inertia would be expected to produce relic diameters determined only by the volume of the droplet, and therefore increasing with increasing pressure and opening time during printing. The suspension with 15 wt.% mass load was chosen for the optimization procedure of the printing parameters due to better visibility of a single droplet relic on the NiO–YSZ substrates. Fig. 3 shows typical set of droplet relics produced at different pressures and opening times from 15 wt.% suspension and sintered at 1100 °C. A statistical analysis of sintered droplet relic area versus opening time and pressure is presented for this suspension in Fig. 4. The error bars represent standard error; typically 5 relics were measured for each combination of pressure and opening time. A systematic increase of area with opening time is observed as expected, but the variation of working pressure over the measured range seems to have a negligible influence on the relic area. We ascribed this effect to the dominance of substrate penetration capillary force over inertia driven spreading within the present volume range. Simultaneously the regularity of the relic shape appeared to be strongly dependent on the pressure applied and less affected by the opening time (see Figs. 5 and 6). Each relic was approximated by an ellipse with area A, major and minor axes a and b, and perimeter p, from which the roundness (R) and circularity (C) were calculated. Roundness is a measure of elongation defined as:

$$R = \frac{4A}{\pi a^2}$$

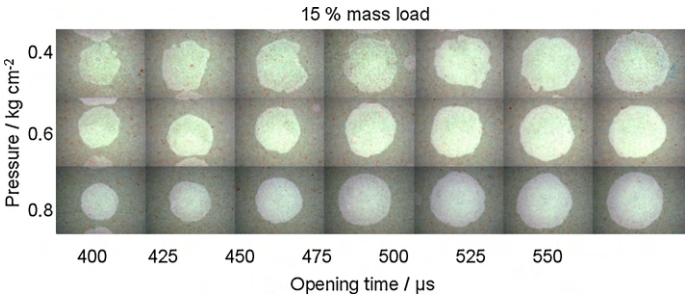

Fig. 3. Representative YSZ droplet relics printed on NiO–YSZ substrate and sintered at 1100 °C, for 0.4, 0.6 and 0.8 kg cm^{-2} pressure and 400–550 μs opening time from 15 wt.% suspension.

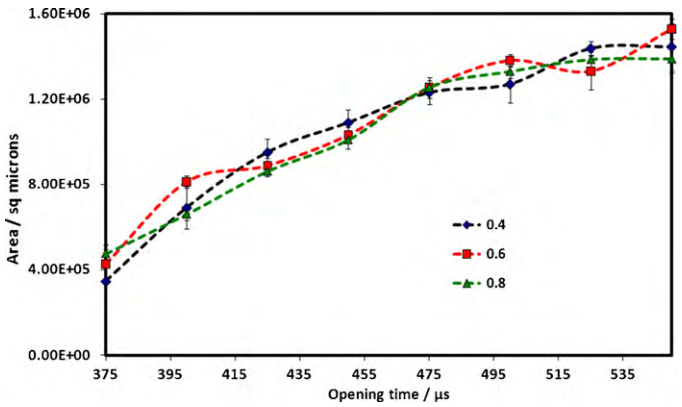

Fig. 4. Sintered droplet relic area versus different opening times and pressures (0.4, 0.6 and 0.8 kg cm^{-2}) for 15 wt.% suspension.

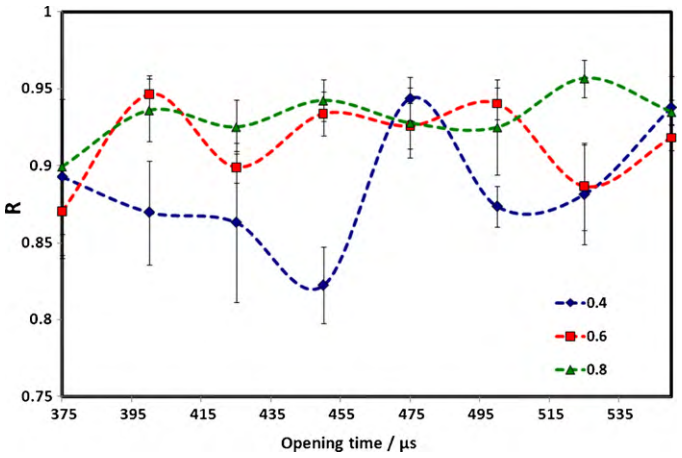

Fig. 5. Sintered droplet relic roundness versus different opening times and pressures (0.4, 0.6 and 0.8 kg cm^{-2}) for 15 wt.% suspension.

where R has a value of 1 for a perfect circle, and decreases with increasing aspect ratio. Circularity is defined as:

$$C = \frac{4\pi A}{p^2}$$

and is also 1 for a perfect circle, decreasing with elongation or edge waviness.

Both roundness and circularity were found to be almost independent of opening time at the highest tested pressure, 0.8 kg cm^{-2}, with average values of 0.92 and 0.75 respectively. As the pressure

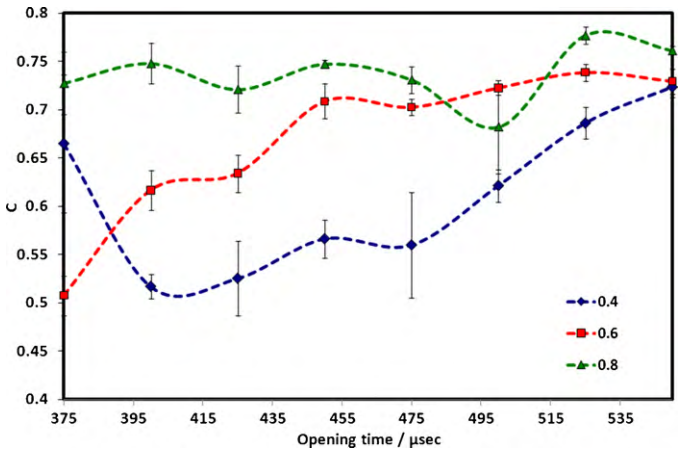

Fig. 6. Sintered droplet relic circularity versus different opening times and pressures (0.4, 0.6 and 0.8 kg cm^{-2}) for 15 wt.% suspension.

was decreased to 0.6 and then 0.4 kg cm^{-2}, the average roundness and circularity both decreased, and the standard deviation increased. The irregularity observed at lower pressures, and at lower opening times, was ascribed to instability of nozzle jetting and the appearance of satellite droplets (which in some cases were observed to impinge on the main drop on the substrate). The best pressure for uniformity was therefore determined to be 0.8 kg cm^{-2}; an opening time of 500 µs was selected to combine uniformity with high mass throughput (further increases in opening time giving only a negligible increase in relic diameter). Similar tests for the 5 wt.% suspension identified 0.6 kg cm^{-2} and 450 µs as the optimum parameters.

3.2. Overlapping parameter optimization

The next step was the optimization of the overlapping parameter (H). The suspension with 15 wt.% powder mass load was printed with different degrees of overlapping on NiO–YSZ substrates using already optimized printing parameters (500 µs opening time and 0.8 kg cm^{-2} pressure). Figs. 7–9 present optical micrographs of the electrolyte coating after sintering at 1100 °C with increasing overlapping (H) from 25% to 60%. Although the increase in H leads to smoothening of the surface, the spreading of the suspension is not sufficient to overcome the formation of axial border ridges even at high overlapping percentages. The porosity of the substrate facilitates this effect by "fixing" the boundary of the droplets on impact with the surface. Additionally the high overlapping percentage has the undesirable effect of increasing the film thickness. Printing two

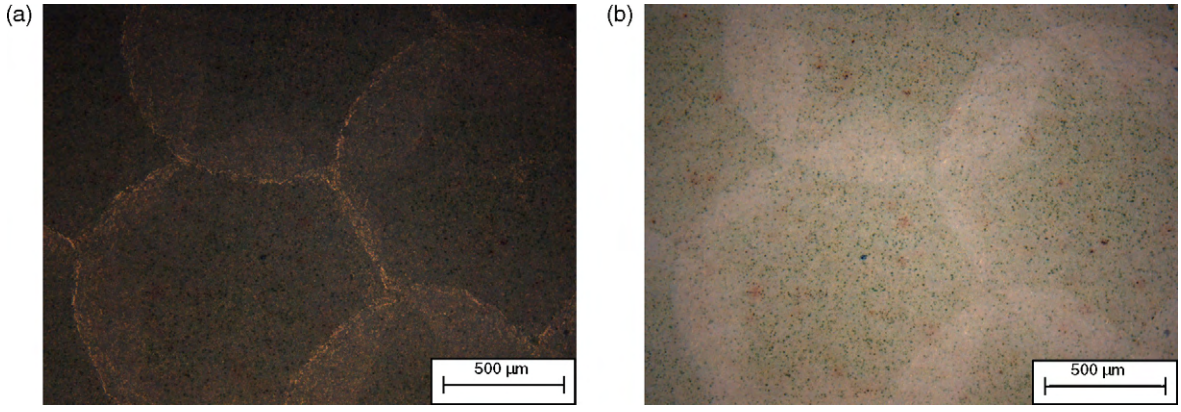

Fig. 7. Optical micrographs (a) dark field and (b) bright field of coatings with 25% of overlapping printed in a hexagonal grid from 15 wt.% mass load suspension as single-layer coating.

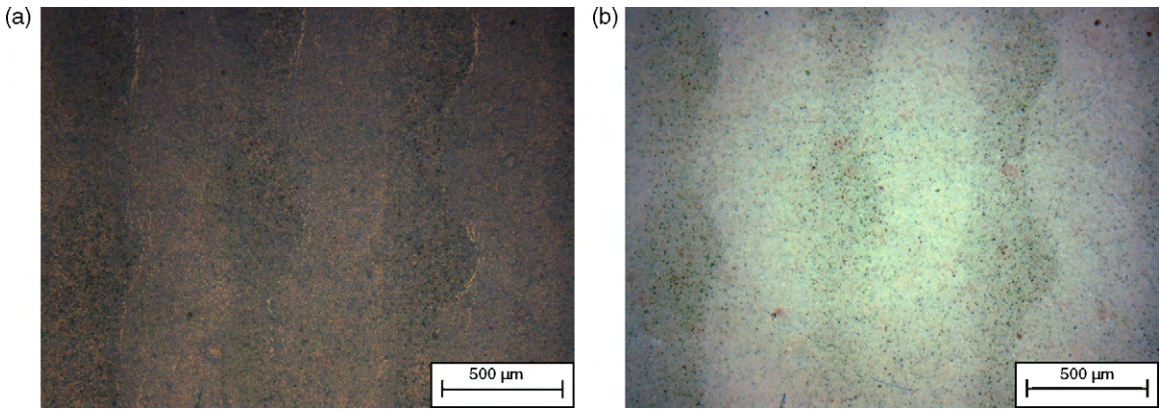

Fig. 8. Optical micrographs (a) dark field and (b) bright field of coatings with 45% of overlapping printed in a hexagonal grid from 15 wt.% mass load suspension as single-layer coating.

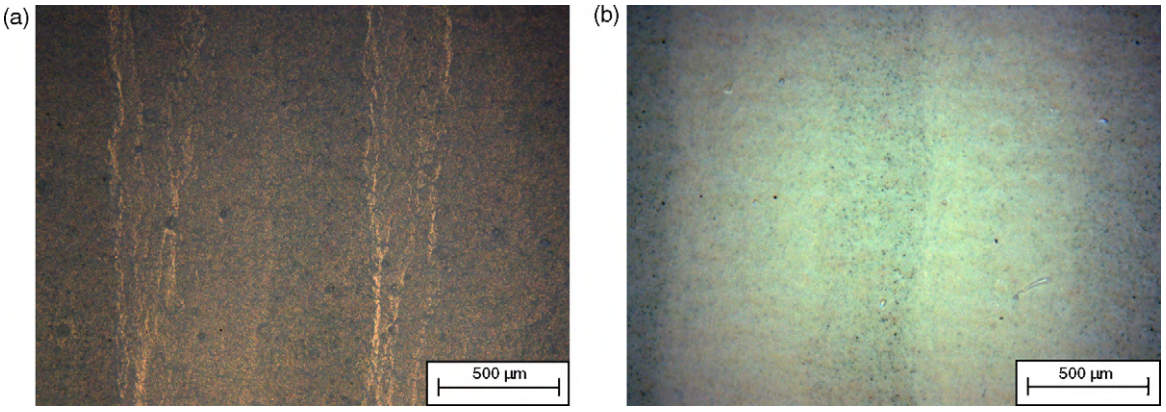

Fig. 9. Optical micrographs (a) dark field and (b) bright field of coatings with 60% of overlapping printed in a hexagonal grid from 15 wt.% mass load suspension as single-layer coating.

layers in succession using moderate overlapping (40%) produced significantly better results, as shown in Fig. 10. In this case the second layer was printed with a half-step offset in the x and y directions. Further surface quality improvement was achieved by utilizing the suspension with lower mass load (5 wt.%) and increasing the number of printed layers. Optical micrographs of a 6-layer coating are shown in Fig. 11. The improved surface smoothness with multi-layer coating was confirmed by surface profilometry. Fig. 12 shows profilometer scans for three of the coatings prepared from the 15 wt.% suspensions. The roughness of the coating prepared from two successive layers with 40% overlapping is lower than for single layers at either 35% or 55% overlapping, with a peak to peak height variation of ±1 μm. This roughness is comparable with the roughness of the NiO–YSZ substrate itself.

3.3. Cell preparation and testing

Based on the optimization results a number of complete coatings were printed on 57 mm × 57 mm NiO–YSZ anode supports and sintered at 1400 °C. Fig. 13(a) and (b) shows SEM micrographs of the surface and cross-section (respectively) of an YSZ electrolyte

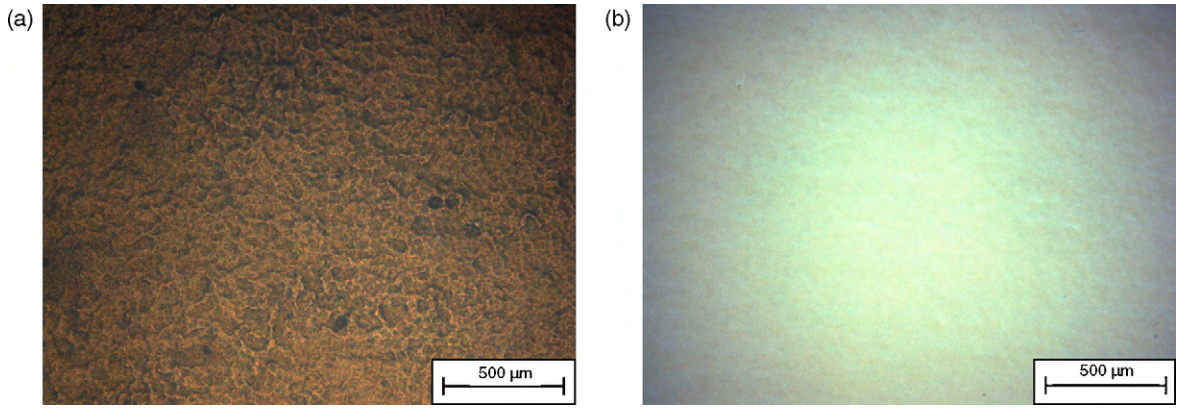

Fig. 10. Optical micrographs (a) dark field and (b) bright field of coatings with 40% of overlapping printed in a hexagonal grid from 15 wt.% mass load suspension as double-layer coating.

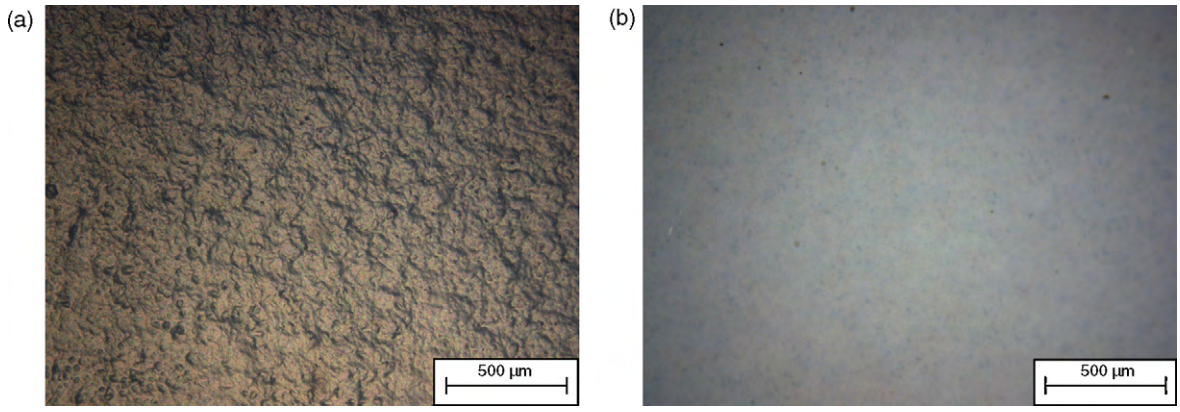

Fig. 11. Optical micrographs (a) dark field and (b) bright field of coatings with 40% of overlapping printed in a hexagonal grid from 5 wt.% mass load suspension as 6-layer coating.

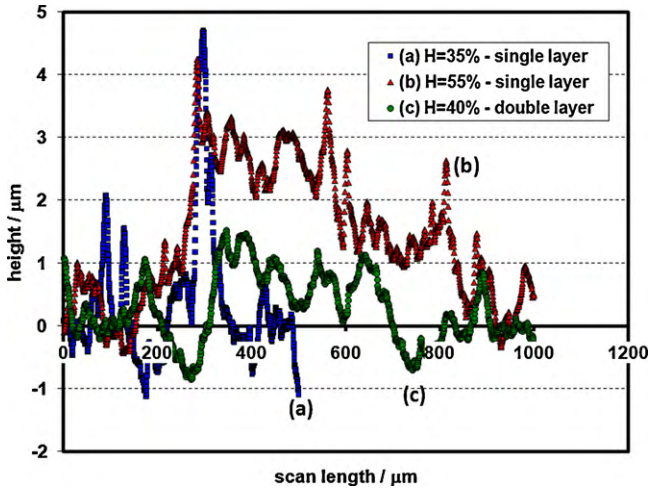

Fig. 12. Surface profilometer scans of three samples printed from the 15 wt.% YSZ suspension and sintered at 1100 °C: (a) single-layer coating, $H = 35\%$; (b) single-layer coating, $H = 55\%$; and (c) double-layer coating, $H = 40\%$.

membrane prepared by inkjet printing of 10 layers from 5 wt.% suspension. It is important to note that the resulting YSZ membrane, as thin as ~5.7–5.9 μm, appears to be highly dense and no open porosity was observed. The film had good interfacial cohesion with the substrate, without any cracking or delamination. Finally, an attempt was made to deposit a thinner YSZ electrolyte coating by reducing the number of layers to 3. Although the desired thickness (~1.5–2.0 μm) and density was achieved, as shown in Fig. 14(a) and (b), some open surface porosity is also apparent, undermining the practicality of such a coating.

Two different test single cells were tested—cell A prepared on a tape-cast anode support without screen-printed interlayer and cell B prepared on the same support with 20 μm thick screen-printed interlayer. In both cases, the electrolyte layer was inkjet printed using 10 layers of the 5 wt.% YSZ suspension, as described above.

Electrical characterization was then performed for each cell. The fuel cell housing was heated to 800 °C and the NiO/YSZ anode cermets were reduced in the presence of sequentially increased hydrogen flow. As anticipated, the open cell voltage (OCV) of the SOFC cell increased steadily with the increase of hydrogen flow. The open cell voltage of 1.01 V was measured for cell A and 1.02 V for cell B operated at 800 °C on hydrogen humidified at 33 °C (fuel: 95% H_2 + 5% H_2O). Although the theoretical OCV value is 1.077 V, the measured values are typical for the gas-tight cells operated without any seals with electrolyte fabricated by both traditional methods and inkjet printing technique [28]. The OCV measurements are consistent with the SEM surface and cross-section appearance (no open porosity). After the cell voltage had stabilized, current–voltage cell performance was measured (see Fig. 15). The cells reached similar power densities of 170 mW cm^{-2} for cell A and 150 mW cm^{-2} for cell B in the humidified hydrogen stream. As-measured power densities are in line with the results reported on cells with similar electrolyte thickness prepared by different techniques. Young et al. [28] reported power densities of 175 mW cm^{-2} measured at 750 °C for cells with 6–12 μm thick inkjet-printed YSZ electrolyte layers. Bao et al. [31] employed an electrostatic powder-coating process to prepare 8 μm thick dense YSZ electrolyte coatings on Ni–YSZ support and reported power densities of 142 mW cm^{-2} measured

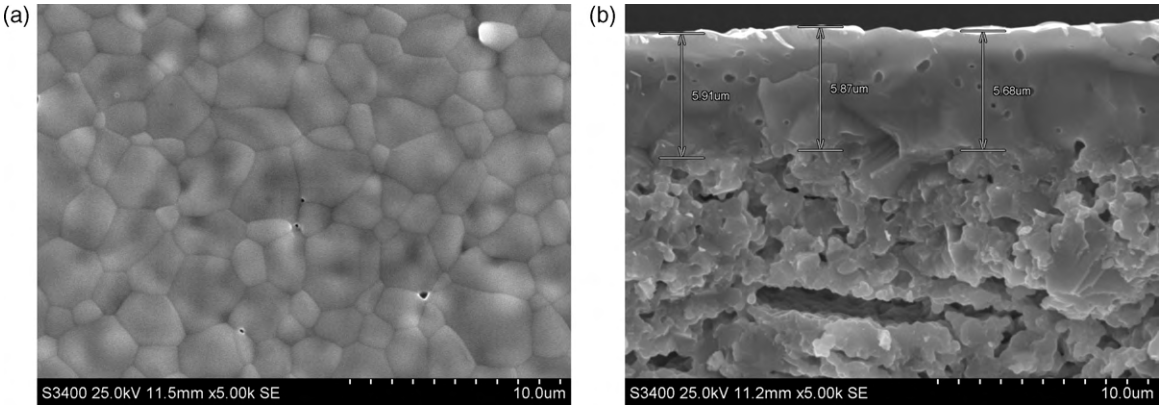

Fig. 13. SEM micrographs of (a) surface and (b) cross-section of a YSZ electrolyte coating prepared by printing 10 layers of 5 wt.% YSZ suspension, sintered at 1400 °C.

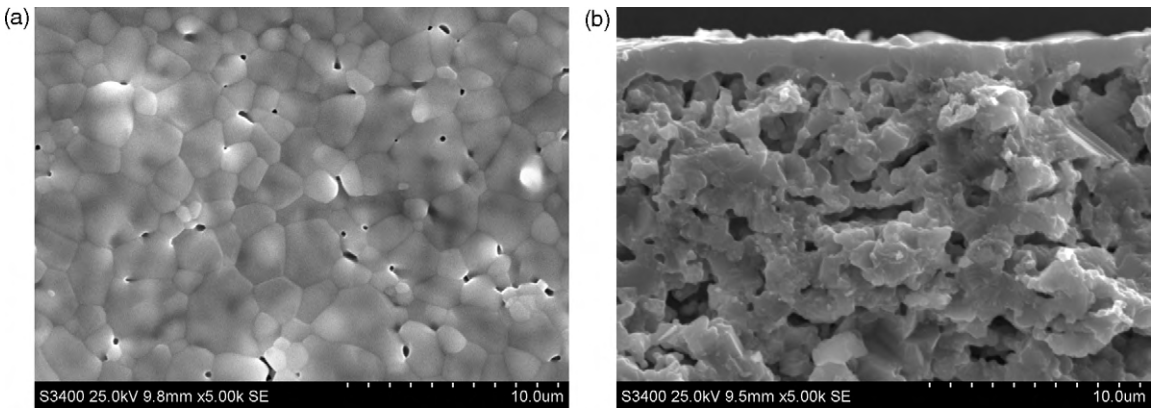

Fig. 14. SEM micrographs of (a) surface and (b) cross-section of a YSZ electrolyte coating prepared by printing 3 layers of 5 wt.% YSZ suspension, sintered at 1400 °C.

at 750 °C. Meng et al. [18] prepared 3 μm thick YSZ electrolyte coatings implementing electron-beam physical vapor deposition combined with a sol infiltration treatment and reported maximum output powder density of 150 mW cm^{-2} obtained at 800 °C.

Fig. 16 shows the impedance spectra for cell A obtained at three different temperatures operated on humidified hydrogen (200 ml min^{-1}). The results have been analyzed with the equivalent circuit model to perform deconvolution of the impedance spectra. Typically processes such as diffusion and absorption occur at lower frequencies while processes such as charge transfer reactions at electrolyte/electrode interfaces occur at higher frequencies [28]. As suggested by Barfordet et al. [32] one or two arcs with frequencies below 100 Hz can be attributed to the concentration polarization for anode-supported cells. At high temperatures (800–850 °C) the overlap between the electrode response and arcs, resulting from concentration polarization, is minimal [32]. Here the two arcs are clearly present for these frequencies at 800 °C and are combined into one arc at lower temperatures −700 and 750 °C (see Fig. 16). The high-frequency arc on Fig. 16 represents the activation polarization of the cell. The summary of the impedance spectra analysis is shown on Fig. 17. The ohmic losses associated with the ohmic resistance of the electrolyte layer and the contact resistances of the electrode/electrolyte interface correspond to less than 65 mΩ resistance and constitute 15% of the cell resistance at 800 °C. The anode concentration polarization appears to be the major loss factor and accounts for 66% of the cell resistance at 800 °C with this percentage increasing at lower temperatures. In order to account for the influence of the interlayer on the concentration polarization losses series of impedance spectra have been measured for both cells at 700 °C and with varying levels of fuel depletion with nitrogen. Keeping the overall fuel flow constant we tested hydrogen concentrations of 20%, 40%, 60% and 100%. The corresponding impedance spectra for cells A and B are presented in Fig. 18. It can be seen that the rate of the increase of polarization losses with the reduction of hydrogen concentration is higher for the cell B indi-

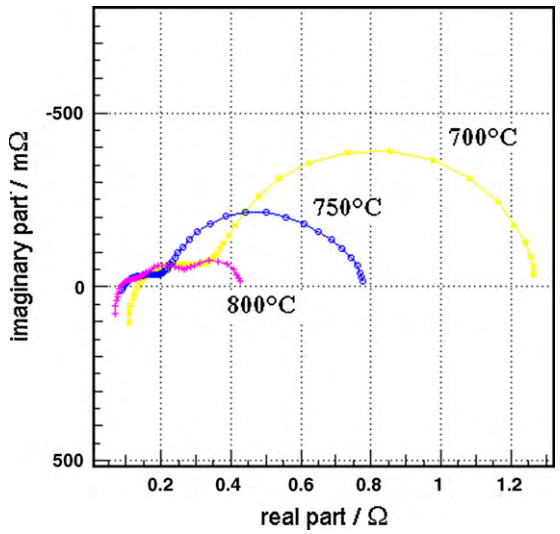

Fig. 16. Impedance spectra of the anode-supported solid oxide fuel cell with an anode functional layer and thin film 8YSZ electrolyte (10 coatings) and with LSM/LSM-3YSZ cathode, measured under open circuit voltage conditions at 800, 750 and 700 °C. Frequency range: from 100 kHz to 100 mHz; cathode gas: air, fuel gas: humidified H_2.

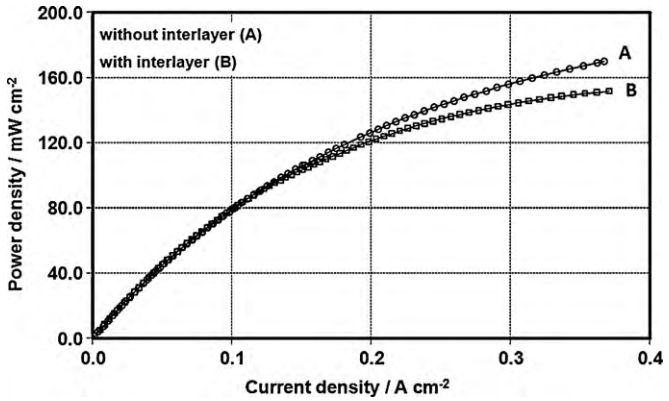

Fig. 15. Power densities of two cells with electrolyte fabricated by the inkjet printing method (A) without Ni–YSZ interlayer, (B) with Ni–YSZ interlayer.

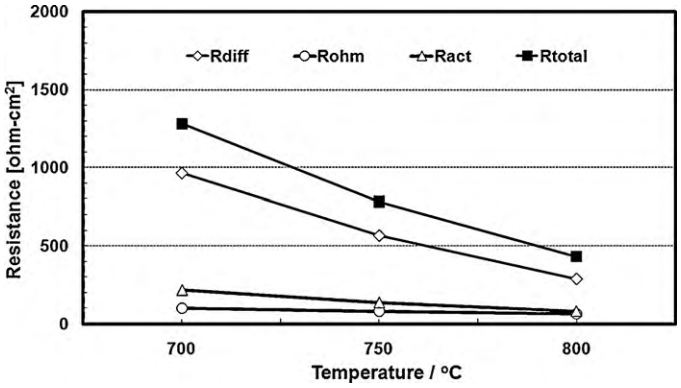

Fig. 17. Summary of the impedance spectra analysis with the temperature where Rdiff represents the diffusion resistance, Rohm represents the ohmic resistance, Ract represents the activation resistance and Rtotal represents the total resistance.

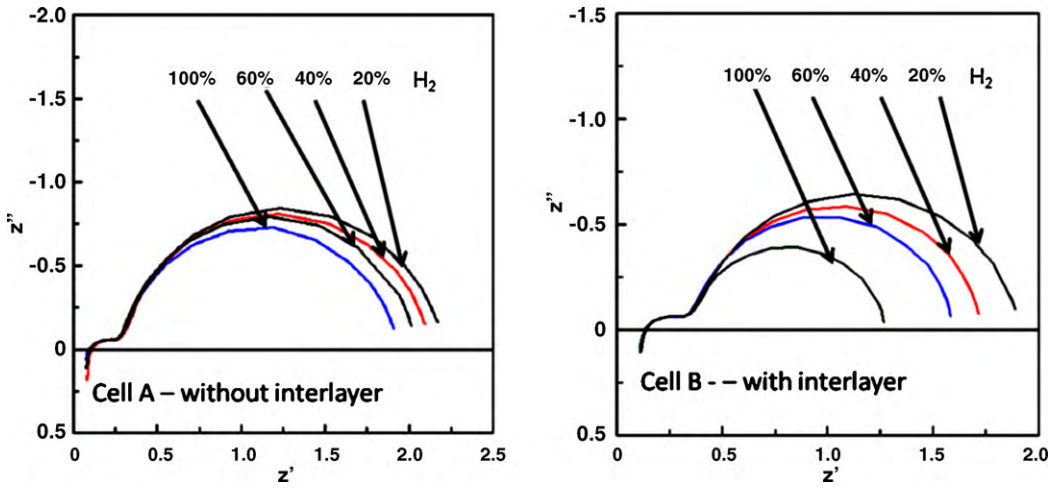

Fig. 18. Impedance spectra for cell A (left) and cell B (right) obtained at 700 °C and at different levels of fuel dilution with nitrogen (hydrogen concentrations 20%, 40%, 60% and 100%).

cating additional losses originating from the gas diffusion in the porous interlayer.

4. Conclusions

Inkjet printing has been successfully demonstrated as a simple and cost-effective technique for the fabrication of thin YSZ electrolytes. Gas-tight YSZ films ~6 μm thick, as evidenced by high open cell voltage (OCV), SEM characterization and cell performance, were deposited on porous Ni–YSZ tape-cast anode supports. SEM revealed no open porosity and excellent interface integrity and electrochemical characterization indicated a stable OCV close to the theoretical value. The *I–V* data are comparable to the results reported in the literature on SOFC with inkjet-printed electrolyte coatings. We believe that the electrolyte thickness can be further reduced by optimizing the printing procedure and suspension properties. The effect of droplet overlapping on surface quality has been studied in detail. The results show that moderate overlapping and repeated coatings can produce a smooth featureless surface without any cracking or delamination. The use of a screen-printed Ni–YSZ interlayer layer led to a small decrease in the cell's maximum power density. It is believed that the factor limiting cell performance is gas diffusion, and work is in progress to improve anode interlayer performance using inkjet printing to deposit layers of controllable porosity.

Acknowledgements

The authors wish to acknowledge EFECTS, "Efficient Environmental-Friendly Electro-Ceramics Coating Technology and Synthesis—EU project FP7-NMP-2007-SMALL-1 grant no. 205854" for financial support. Dr. R.I. Tomov would like to acknowledge partial financial support from the EPSRC project 'SUPERGEN XIV—Delivery of sustainable hydrogen'.

References

[1] N.Q. Minh, J. Am. Ceram. Soc. 76 (3) (1993) 563–588.
[2] S. Singhal, Solid State Ionics 135 (1–4) (2000) 305–313.
[3] Z.P. Shao, S.M. Haile, J. Ahn, P.D. Ronney, Z.L. Zhan, S.A. Barnett, Nature 435 (2005) 795–798.
[4] K. Choy, W. Bai, S. Charojrochkul, B.C.H. Steele, J. Power Sources 71 (1998) 361–369.
[5] A. Weber, E. Ivers-Tiffee, J. Power Sources 127 (2004) 273–283.
[6] S. de Souza, S.J. Visco, L.C. De Jonghe, Solid State Ionics 98 (1997) 57–61.
[7] I.R. Gibson, G.P. Dransfield, J.T.S. Irvine, J. Eur. Ceram. Soc. 18 (1998) 661–667.
[8] X.S. Xin, Z. Lu, X.Q. Huang, X.Q. Sha, Y.H. Zhang, W.H. Su, Mater. Res. Bull. 41 (2006) 1319–1329.
[9] X.J. Chen, K.A. Khor, S.H. Chan, L.G. Yu, Mater. Sci. Eng. A335 (2002) 246–252.
[10] S.P. Jiang, S.H. Chan, J. Mater. Sci. 39 (2004) 4405.
[11] C. Song, Catal. Today 77 (2002) 17–49.
[12] B.C.H. Steele, A. Heinzel, Nature 414 (2001) 345–352.
[13] Y.J. Leng, S.H. Chan, S.P. Jiang, K.A. Khor, Solid State Ionics 170 (2004) 9–15.
[14] J. Will, A. Mitterdorfer, C. Kleinlogel, D. Perednis, L.J. Gauckler, Solid State Ionics 131 (2000) 79–96.
[15] S. de Souza, S.J. Visco, L.C. De Jonghe, J. Electrochem. Soc. 144 (3) (1997) L35–L37.
[16] A. Nagata, H. Okayama, Vacuum 66 (2002) 523–529.
[17] K.L. Choy, Chemical vapour deposition of coatings, Prog. Mater. Sci. 48 (2) (2003) 57–170.
[18] B. Meng, X. He, Y. Sun, M. Li, Mater. Sci. Eng. B 150 (2008) 83–88.
[19] T. Fukui, S. Ohara, K. Murata, H. Yoshida, K. Miura, T. Inagaki, J. Power Sources 106 (2002) 142–145.
[20] R.R. Peng, C.R. Xia, X.Q. Liu, D.K. Peng, G.Y. Meng, Solid State Ionics 152–153 (2002) 561–565;
X. Ge, X. Huang, Y. Zhang, Z. Lua, J. Xua, K. Chen, D. Dong, Z. Liu, J. Miao, W. Su, J. Power Sources 159 (2006) 1048–1050.
[21] P. Bohac, L. Gauckler, Solid State Ionics 119 (1999) 317–321.
[22] S. Uhlenbruck, T. Hoppe, H.P. Buchkremer, D. Stöver, J. Ceram. Process. Res. 7 (3) (2006) 214–220.
[23] F. Mauvy, P. Lenormand, C. Lalanne, F. Ansart, J.M. Bassat, J.C. Grenier, J. Power Sources 171 (2007) 783–788.
[24] Y.Y. Chen, W.-C.J. Wei, Solid State Ionics 177 (2006) 351–357.
[25] T. Mouganie, B.A. Glowacki, J. Mater. Sci. 41 (2006) (2006) 8257–8264.
[26] D. Pecha, M. Bruneta, P.-L. Tabernab, P. Simonb, N. Fabrea, F. Mesnilgrentea, V. Conederaa, H. Duroua, J. Power Sources 195 (2010) 1266–1269.
[27] T. Mouganie, M.A. Moram, J. Sumner, B.A. Glowacki, B. Schoofs, I. van Driessche, S. Hoste, J. Sol–Gel Sci. Technol. 36 (2005) 87–94.
[28] D. Young, A.M. Sukeshini, R. Cummins, H. Xiao, M. Rottmayer, T. Reitz, J. Power Sources 184 (2008) 191–196.
[29] A.M. El-Toni, T. Yamaguchi, S. Shimizu, Y. Fujishiro, M. Awano, J. Am. Ceram. Soc. 91 (1) (2008) 346–349.
[30] A.K. Maiti, B. Rajender, Mater. Sci. Eng. A 333 (2002) 35–40.
[31] W. Bao, W. Zhu, G. Zhu, J. Gao, G. Meng, Solid State Ionics 176 (2005) 669–674.
[32] R. Barford, A. Hagen, S. Ramousse, P.V. Hendriksen, M. Mogensen, Fuel Cells 2 (2006) 141–145.